Stem Cell Reports
Article

ISSCR

OPEN ACCESS

Primary Cilia Are Dysfunctional in Obese Adipose-Derived Mesenchymal Stem Cells

Andreas Ritter,[1] Alexandra Friemel,[1] Nina-Naomi Kreis,[1] Samira Catharina Hoock,[1] Susanne Roth,[1] Ulrikke Kielland-Kaisen,[1] Dörthe Brüggmann,[1] Christine Solbach,[1] Frank Louwen,[1,2] and Juping Yuan[1,2,*]
[1]Department of Gynecology and Obstetrics, School of Medicine, J. W. Goethe University, Theodor-Stern-Kai 7, 60590 Frankfurt, Germany
[2]Co-senior author
*Correspondence: yuan@em.uni-frankfurt.de
https://doi.org/10.1016/j.stemcr.2017.12.022

SUMMARY

Adipose-derived mesenchymal stem cells (ASCs) have crucial functions, but their roles in obesity are not well defined. We show here that ASCs from obese individuals have defective primary cilia, which are shortened and unable to properly respond to stimuli. Impaired cilia compromise ASC functionalities. Exposure to obesity-related hypoxia and cytokines shortens cilia of lean ASCs. Like obese ASCs, lean ASCs treated with interleukin-6 are deficient in the Hedgehog pathway, and their differentiation capability is associated with increased ciliary disassembly genes like *AURKA*. Interestingly, inhibition of Aurora A or its downstream target the histone deacetylase 6 rescues the cilium length and function of obese ASCs. This work highlights a mechanism whereby defective cilia render ASCs dysfunctional, resulting in diseased adipose tissue. Impaired cilia in ASCs may be a key event in the pathogenesis of obesity, and its correction might provide an alternative strategy for combating obesity and its associated diseases.

INTRODUCTION

The increase in the prevalence of obesity poses a global challenge. Obesity leads frequently to metabolic syndromes like diabetes mellitus type 2 and cardiovascular diseases (O'Neill and O'Driscoll, 2015). Moreover, it is associated with diverse aspects of malignancy (Donohoe et al., 2017). The molecular pathways linking obesity with these diseases are relevant to subclinical chronic inflammation, insulin resistance, defective immunomodulation, and increased invasion and metastasis of tumor cells (Freitas Lima et al., 2015; Donohoe et al., 2017). Adipose tissue in the obese state is characterized by adipocyte hypertrophy, local hypoxia, increased infiltrating immune cells, enhanced pro-inflammatory adipokines/chemokines, decreased adipogenesis, and impaired angiogenesis (Kloting and Bluher, 2014; Patel and Abate, 2013). The molecular mechanisms underlying the development of obesity and its associated diseases are still incomplete.

Adipose-derived mesenchymal stem cells (ASCs), a crucial cell population of adipose tissue, have multiple functions including their potent differentiation capability responsible for adipogenesis and angiogenesis (Gimble et al., 2007; Cawthorn et al., 2012). These cells control the local and systemic environment by immunomodulation and damage repair through direct cell-cell interaction and secretion of numerous cytokines and chemokines (Cawthorn et al., 2012; Strong et al., 2015; Donohoe et al., 2017). Obesity reduces the differentiation capability of ASCs and alters their immune phenotype (Serena et al., 2016; Pachon-Pena et al., 2011). Impaired obese ASCs contribute further to the development of obesity by affecting adipose tissue remodeling, inducing hypoxia, and secreting pro-inflammatory cytokines (Badimon and Cubedo, 2017). Obese-derived ASCs promote also tumor development via multiple mechanisms including facilitating the infiltration of T cells and macrophages (Donohoe et al., 2017; Strong et al., 2016). The mechanisms underlying the ASC impairment in obesity are, however, not defined.

ASCs respond to environmental cues through their surface receptors and especially a sensor organelle termed the primary cilium. The primary cilium, an antenna-like cellular protrusion, is present on almost all vertebrate cells, mediating numerous signals from the extracellular environment via various signal transduction pathways (Malicki and Johnson, 2017). In particular, it is indispensable for the Hedgehog (Hh) signaling in mammals (He et al., 2017; Pak and Segal, 2016). Structurally, the primary cilium comprises a microtubule (MT)-based axoneme sheathed by the ciliary membrane and is nucleated from the basal body developed from the mother centriole (Hilgendorf et al., 2016). Functionally, being coupled with the cell cycle, primary cilia mediate an astonishing diversity of cellular functions including cell growth and development and cellular homeostasis (Malicki and Johnson, 2017; Goto et al., 2016). In fact, its malfunction leads to various human developmental disorders, commonly known as ciliopathies (Sanchez and Dynlacht, 2016).

Interestingly, it has been reported that the primary cilium is crucial for maintaining stemness, defining the cell phenotype, and functioning as a signal sensor and transducer in stem/progenitor cells (Forcioli-Conti et al., 2015; Dalbay et al., 2015; Bodle and Loboa, 2016).

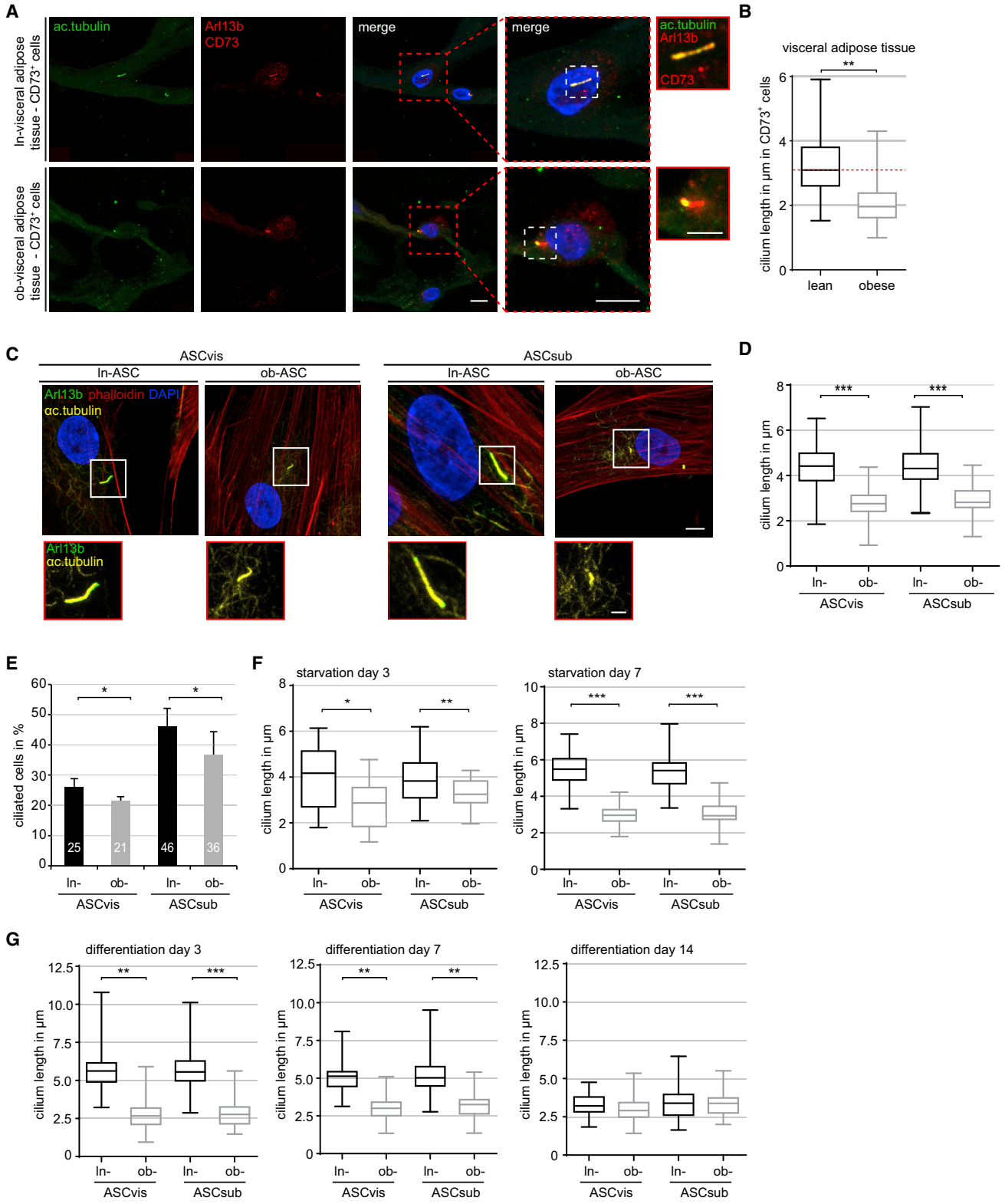

Figure 1. Cilia Are Shortened in Obese ASCs

(A) Visceral adipose tissue sections from three lean (ln) and three obese donors (ob) were stained as indicated. Representatives are shown. Scale bar: 7.5 µm. Inset scale bar: 3 µm.

(legend continued on next page)

Considering the multiple vital roles of ASCs, we hypothesized their involvement in the pathogenesis of obesity. In particular, we were interested in if and how primary cilia of ASCs function in the obese state. We show here that cilia are impaired in their morphology and functionalities, which renders ASCs from obese donors dysfunctional.

RESULTS

Shortened Primary Cilia in ASCs from Obese Donors

To investigate if obesity affects the primary cilium in ASCs, we collected visceral adipose tissues from three female control donors (BMI [body mass index] <25) and three female obese donors (BMI >35) undergoing selective cesarean section at term. The reproductive state has been reported to hardly impact the features of human ASCs (Ng et al., 2009). Fluorescence immunohistochemistry was performed with adipose tissue sections by co-staining with antibodies against the cilium markers Arl13b and acetylated α-tubulin and against CD73, a typical ASC surface marker (Dominici et al., 2006). Interestingly, microscopic evaluation revealed that the cilium length was significantly reduced in obese visceral adipose tissues relative to normal visceral adipose tissues (Figure 1A). Further analysis showed that the mean length of cilia was 3.27 ± 0.96 μm in normal adipose tissues, whereas it was only 2.08 ± 0.64 μm in obese visceral adipose tissues (Figure 1B), a reduction of 36%.

To further characterize primary cilia, we isolated ASCs from subcutaneous and visceral adipose tissues (Ritter et al., 2015) of the same female donors with normal weight (BMI <25, ln-ASCs, for ASCs from normal lean controls) or with obesity (BMI >35, ob-ASCs, for ASCs from obese donors). The clinical information of donors is summarized in Table S1. As depicted in Table S2, cell purity was evaluated by examining typical cell surface markers for mesenchymal stem cells described by the Society of Cellular Therapy (Dominici et al., 2006).

To compare the cilium size between ob-ASCs and ln-ASCs, cells were stained for acetylated α-tubulin and Arl13b, the actin filament marker phalloidin, and DNA followed by microscopic analysis. In line with the observation from primary adipose tissue sections, the primary cilium was greatly shortened in ob-ASCs (Figure 1C). The mean length of primary cilia was 4.43 ± 0.91 μm in visceral ln-ASCs, whereas it was only 2.76 ± 0.60 μm in visceral ob-ASCs (Figure 1D), a reduction of 38%. A decrease of 33% of the cilium length was also observed in subcutaneous ob-ASCs relative to ln-ASCs (Figure 1D, 2.93 ± 0.57 versus 4.36 ± 0.94 μm). Compared with the length in primary adipose tissues (Figure 1B), the cilia were slightly longer in isolated ASCs (Figure 1D), probably ascribed to ASCs' monolayer culture condition. While 25% of visceral ln-ASCs were ciliated, the primary cilium was present in 46% of subcutaneous ln-ASCs (Figure 1E), suggesting that these two types of ASCs differ in their response to extracellular stimuli. The ciliated populations were decreased in both types of ob-ASCs, compared with their counterpart ln-ASCs (Figure 1E). Subsequent analysis showed that primary cilia in the majority of ln-ASCs were 4–6 μm in length, whereas they were 2–4 μm in ob-ASCs (Figure S1A). Thus, the cilium length and ciliated-cell population were reduced in ASCs derived from obese donors.

Serum Starvation Barely Alters the Length of Cilia in ob-ASCs

Cells assemble their cilia in response to cellular quiescence (Goto et al., 2016), induced, for example, by serum starvation. To determine if shortened cilia are able to dynamically elongate their length, ASCs were cultured without serum for up to 7 days. At days 3 and 7, cells were stained for cilium markers. Microscopic analysis demonstrated that the cilium length remained relatively constant in ob-ASCs, whereas cilia in ln-ASCs extended their length during the starvation course (Figures 1F and S1B). Compared with ln-ASCs, ciliated populations were reduced

(B) The cilium length in (A) was measured using Arl13b staining as cilium marker. The results are from three experiments (n = 80–85 cilia for each group) and presented as box plots. Red dashed line indicates the cilium median length of $CD73^+$ cells in lean visceral adipose tissue.

(C) Lean or obese ASCs (ln-ASCs versus ob-ASCs) from visceral (ASCvis) and subcutaneous adipose tissues (ASCsub) were stained as indicated. Representatives are shown. Scale bar: 4.5 μm. Inset scale bar: 2 μm.

(D) Evaluation of the cilium length in ASCs. The results are based on six experiments using ASCs from six obese and six lean donors (n = 174–183 cilia for each group).

(E) Ciliated ASCs were evaluated and presented as mean ± SEM (n = 600 cells, pooled from six experiments).

(F) ASCs were starved for up to 7 days and stained as in (C) for evaluating the cilium length at day 3 (left) and day 7 (right). The results are based on three experiments (n = 103–110 cilia for each condition).

(G) ASCs were induced into osteogenic differentiation for up to 14 days, and stained as in (C) for the evaluation of the cilium length at day 3 (left), day 7 (middle), and day 14 (right). The results are from three experiments (n = 107–124 cilia for each condition).

Box and whisker plots were used to show the median and the minimal to maximal range of the values in (B), (D), (F), and (G). Unpaired Mann-Whitney U test for (B), (D), (F), and (G). Student's t test for (E). *p < 0.05, **p < 0.01, ***p < 0.001.

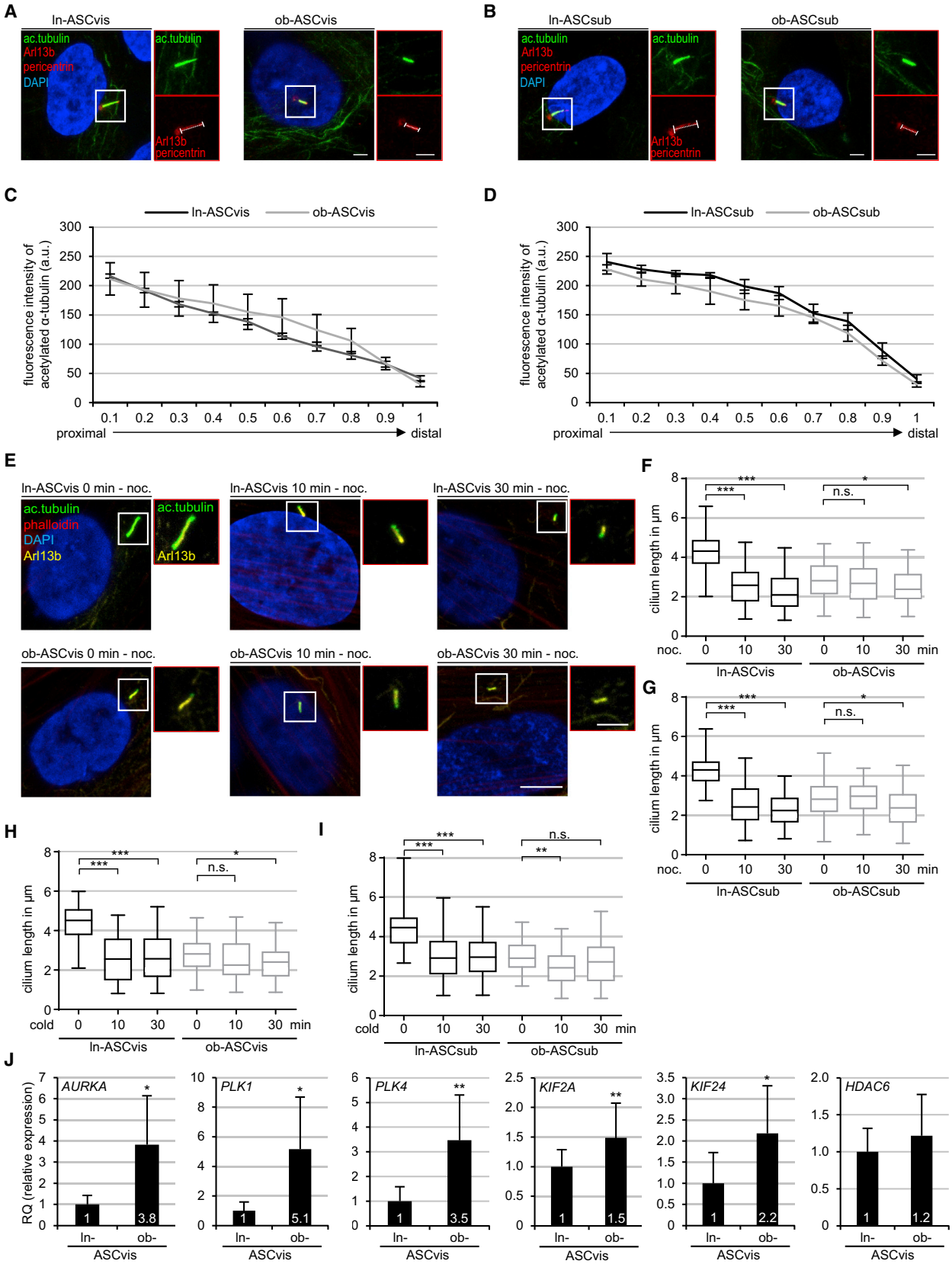

(legend on next page)

in both visceral and subcutaneous ob-ASCs at day 7 (Figure S1C). Moreover, after 7 days of starvation, 74% visceral and 87% subcutaneous ln-ASCs displayed their cilium length in a range of 4–6 μm, accompanied by 26% visceral and 13% subcutaneous ln-ASCs with a cilium length of 6–8 μm (Figure S1D, top). By contrast, 81% visceral and 89% subcutaneous ob-ASCs showed cilia with 2–4 μm and only small populations displayed cilia with 4–6 μm (Figure S1D, bottom). Unlike ln-ASCs, serum starvation is thus incapable of triggering ob-ASCs to assemble their cilia, albeit there is an increase in their ciliated population.

Shortened Cilia of ob-ASCs Are Unable to Respond Dynamically to Differentiation Stimuli

The primary cilium undergoes a dynamic length change in ASCs during differentiation (Forcioli-Conti et al., 2015; Dalbay et al., 2015), suggesting that the cilium size is linked to this potential. To determine if the shortened cilia were able to undergo this dynamic alteration in ob-ASCs, cells were subjected to osteogenic differentiation medium for 14 days. At days 3, 7, and 14, cells were stained for cilium markers followed by microscopic evaluation. As expected, primary cilia in ln-ASCs were elongated upon induction of osteogenic differentiation at day 3 (Figure 1G, left), kept their length until day 7 (Figure 1G, middle), and resorbed them as cells were in the late stages of differentiation at day 14 (Figure 1G, right). On the contrary, cilia in ob-ASCs were hardly changed and retained their reduced length throughout the differentiation process (Figures 1G and S2A). In-depth analysis of the cilium length further pointed to this notion (Figure S2B). The shortened cilia in ob-ASCs are non-dynamic even during differentiation, implying that primary cilia in ob-ASCs are inefficient at responding to extracellular stimuli.

Decreased Dynamics of the Axoneme in ob-ASCs

Cilium stability is associated with post-modifications of axonemal MTs like α-tubulin acetylation (Janke and Bulinski, 2011), which promotes the primary cilium assembly (Forcioli-Conti et al., 2016). To investigate this post-modification of axonemal MTs, a line-scan analysis of fluorescent acetylated α-tubulin was performed from the proximal base to the distal tip of cilia in stained ASCs normalized to the cilium length marked by Arl13b staining in visceral (Figure 2A) and subcutaneous ASCs (Figure 2B), as described (He et al., 2014). The levels of α-tubulin acetylation in cilia were comparable between ln-ASCs and ob-ASCs from both visceral and subcutaneous adipose tissues (Figures 2C and 2D), suggesting that the stability of axonemal MTs is hardly affected in ob-ASCs, despite their shortened length. Notably, the content of acetylated α-tubulin was obviously higher in subcutaneous ASCs relative to visceral ASCs (Figures 2C and 2D), indicating that primary cilia in subcutaneous ASCs may be more stable than in ASCs from the visceral adipose depot.

To explore the dynamics of axonemal MTs in ob-ASCs, cells were treated with nocodazole for 30 min to induce MT depolymerization. At 0, 10, and 30 min, cells were stained for acetylated α-tubulin, Arl13b, phalloidin, and DNA. The axonemal length in ln-ASCs altered dynamically upon addition of nocodazole, whereas it changed only slightly in ob-ASCs (Figure 2E). The length of acetylated α-tubulin-labeled axonemal MTs was remarkably reduced by 41% at 10 min and 48% at 30 min in visceral ln-ASCs (Figure 2F). By contrast, the decrease in the axonemal length was only 4% at 10 min and 14% at 30 min in visceral ob-ASCs treated with nocodazole (Figure 2F). Like visceral ob-ASCs, subcutaneous ob-ASCs were also unable to depolymerize their axonemal MTs, whereas subcutaneous ln-ASCs effectively disassembled their cilia in the presence of

Figure 2. Less Dynamic Axoneme and Enhanced Deciliation Genes in ob-ASCs

(A and B) Visceral (A) and subcutaneous ln-ASCs and ob-ASCs (B) were stained for evaluating the fluorescence intensity of axonemal acetylated microtubules (green channel) from the axonemal base to the distal tip, normalized to the corresponding cilium length (Arl13b staining, red channel). Representatives are shown. Insets depict the staining of acetylated α-tubulin (right top) and pericentrin/Arl13b (right bottom). Scale bars: 3 μm.

(C and D) The fluorescence intensities of visceral (C) and subcutaneous (D) axonemal acetylated microtubules are shown. The data are from three experiments (n = 30 cilia for each condition) and presented as mean ± SEM.

(E–G) ASCs were treated with 10 μM nocodazole (noc.) for 30 min and stained as indicated. Representatives are shown (E). Scale bar: 7.5 μm. Inset scale bar: 3 μm. The length of acetylated α-tubulin-labeled axonemes was evaluated. The results are based on three experiments with ASCs from three lean and three obese donors (n = 97–108 cilia for each time point) in visceral (F) and subcutaneous ASCs (G).

(H and I) ASCs were cold treated for 30 min and stained for evaluating the length of acetylated α-tubulin-labeled axonemes. The data are based on three experiments with ASCs from three lean and three obese donors (n = 89–96 cilia for each time point). The cilium length is shown for visceral (H) and subcutaneous ASCs (I).

(J) The gene levels of deciliation molecules. The data are based on three experiments and presented as mean ± SEM. RQ, relative quantification of gene expression.

Box and whisker plots were used to show the median and the minimal to maximal range of the values in (F)–(I). Unpaired Mann-Whitney U test for (C), (D), and (F)–(I). Student's t test for (J). *p < 0.05, **p < 0.01, ***p < 0.001.

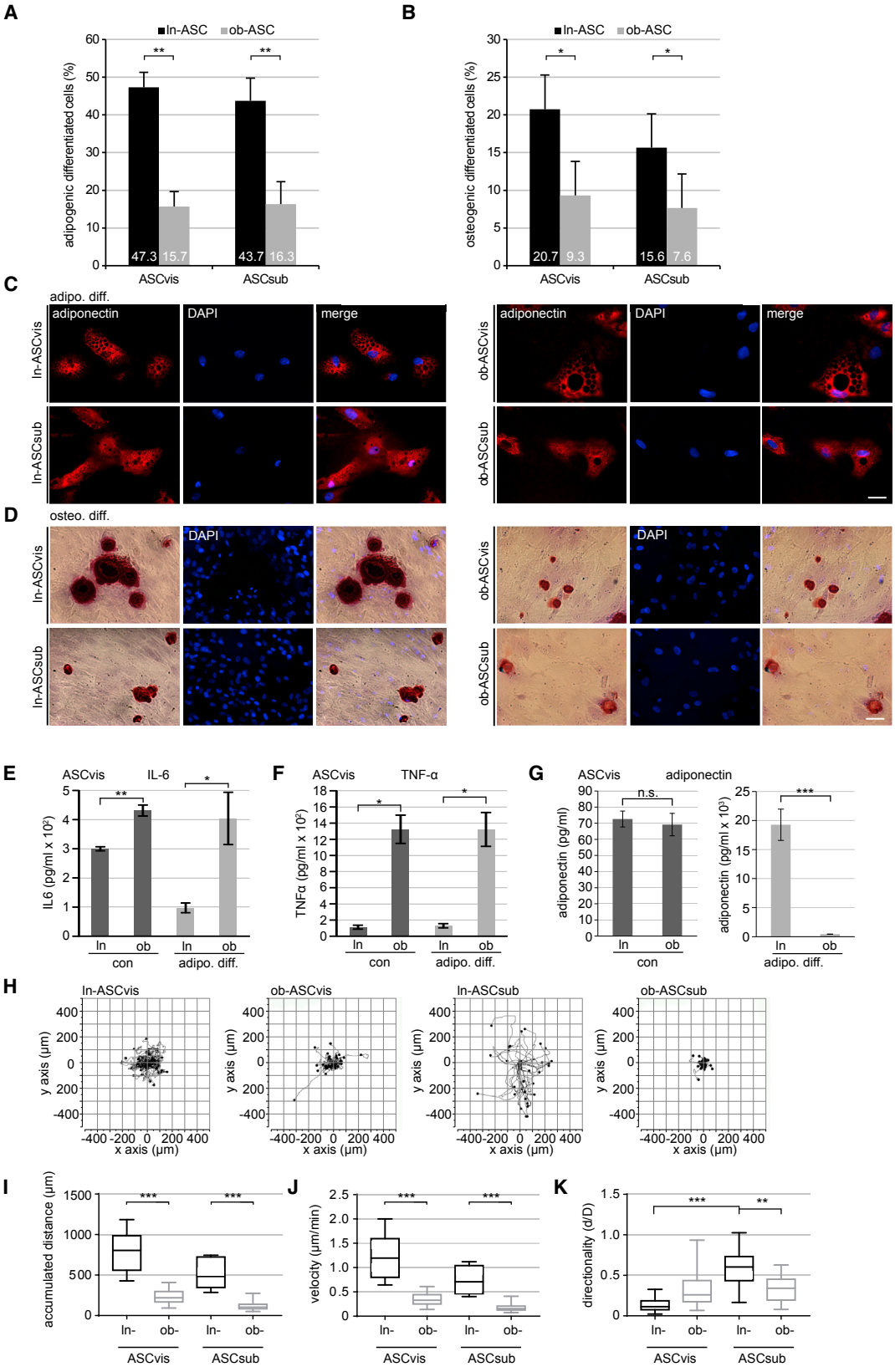

(legend on next page)

nocodazole (Figure 2G). This observation was further corroborated by the cold treatment assay: while visceral and subcutaneous ln-ASCs responded to the exposure to 4°C by effectively destabilizing their axonemal MTs, ob-ASCs barely shortened their axonemal length (Figures 2H and 2I). These data suggest that, unlike ln-ASCs, ob-ASCs from both depots are less capable of dynamically destabilizing their axonemal MTs upon nocodazole or cold treatment.

Cell-Cycle Profile Is Scarcely Changed in ob-ASCs

The length of the primary cilium is coupled with the cell cycle (Goto et al., 2016). To explore if proliferation-related deciliation accounts for these shortened cilia in ob-ASCs, viability assays, western blot analysis, G2/M population evaluation, and staining of the mitotic marker phosphohistone H3 were performed. No significant differences were observed between ln-ASCs and ob-ASCs at their early passages used in this work (Figures S3A–S3D), suggesting that shortened cilia in ob-ASCs are not the consequence of an enhanced cell proliferation.

Increased Deciliation Genes in ob-ASCs

We next analyzed important genes related to ciliogenesis. Compared with visceral ln-ASCs, three mitotic kinase genes, *AURKA* (Aurora kinase A), *PLK1* (Polo-like kinase 1), and *PLK4,* and two depolymerase genes, *KIF2A* and *KIF24*, crucial regulators for both mitosis and deciliation (Sanchez and Dynlacht, 2016; Korobeynikov et al., 2017), were significantly enhanced in visceral ob-ASCs (Figure 2J). Increased *PLK1*, *PLK4*, and *KIF2A* were also observed in subcutaneous ob-ASCs (Figure S3E). The gene expression of *HDAC6*, a deacetylase important for ciliary disassembly (Forcioli-Conti et al., 2016), was more strongly enhanced in subcutaneous ob-ASCs (Figure S3E) than in visceral ob-ASCs (Figure 2J). The results suggest that multiple molecules related to cilium biogenesis are deregulated in ob-ASCs.

ob-ASCs Differentiate Poorly and Migrate Slowly with Altered Secretion of Adipokines

The cilium size is tightly linked to differentiation of ASCs/progenitor cells (Strong et al., 2015; Zhu et al., 2009). To investigate if the shortened cilia impact this capability of ob-ASCs, cells were subjected to adipogenic or osteogenic differentiation for 14 or 21 days, respectively. For microscopic evaluation, cells were stained for adiponectin, characteristic of adipocytes, or alizarin red S to visualize calcific deposition typical for osteogenic lineage. Relative to ln-ASCs, ob-ASCs, regardless of their depots, showed an impaired capability of adipogenic (Figures 3A and 3C) and osteogenic differentiation (Figures 3B and 3D). Moreover, compared with ln-ASCs, ob-ASCs secreted more interleukin-6 (IL-6) and tumor necrosis factor alpha (TNF-α) before and after adipogenic differentiation (Figures 3E and 3F), but produced significantly less adiponectin after differentiation (Figure 3G).

The primary cilium is involved in controlling cell motility (Malicki and Johnson, 2017). To address this issue, time-lapse microscopy was performed (Ritter et al., 2015). We tracked single ASCs up to 12 hr (Figure 3H) and evaluated the movement of individual cells (Wu et al., 2016). The accumulated distance and the velocity of ob-ASCs were significantly decreased compared with ln-ASCs (Figures 3I and 3J). Relative to ln-ASCs, visceral as well as subcutaneous ob-ASCs had a reduced velocity of 72% (1.21 ± 043 versus 0.34 ± 0.11 μm/min) and 77% (0.73 ± 0.26 versus 0.17 ± 0.07 μm/min) (Figure 3J), respectively. As reported (Ritter et al., 2015), subcutaneous ln-ASCs displayed a remarkable intrinsic directionality, while visceral ln-ASCs moved themselves almost randomly (Figure 3K). In comparison with subcutaneous ln-ASCs, ob-ASCs reduced this ability (Figure 3K). The shortened cilia are thus associated with ASC poor differentiation and slow migration, accompanied by increased secretion of pro-inflammatory cytokines IL-6 and TNF-α and decreased production of anti-inflammatory adipokine adiponectin.

Deficient Hh Signaling in ob-ASCs

The Hh signaling pathway is crucial for differentiation (Bodle and Loboa, 2016), and its activation recruits Smoothened (Smo) and glioma-associated oncogene homolog 1 (Gli1) to the cilium (Pak and Segal, 2016). To study

Figure 3. Impaired Differentiation, Migration, and Adipokine Secretion of ob-ASCs

(A–D) Adipogenic (adipo. diff.) (A) and osteogenic differentiation (osteo. diff.) (B) were evaluated by adiponectin and alizarin red S staining, respectively. The results are presented as mean ± SEM in visceral and subcutaneous ASCs (n = 300 cells for each condition, pooled from three experiments). Example images are shown in (C) and (D), respectively. Scale bars: 25 μm.

(E–G) Seventy-two hour supernatants before and after adipogenic differentiation were collected for the evaluation of IL-6 (E), TNF-α (F), and adiponectin (G). The results are from three experiments and presented as mean ± SEM.

(H–K) Analysis of ASC motility. Representative trajectories are depicted for individual cells (H, n = 30 cells in each group). The accumulated distance (I), the velocity (J), and the directionality (K) of ASC migration are shown (n = 90 cells pooled from three experiments).

Box and whisker plots were used to show the median and the minimal to maximal range of the values in (I)–(K). Unpaired Mann-Whitney U test for (I)–(K). Student's t test for (A), (B), and (E)–(G). *p < 0.05, **p < 0.01, ***p < 0.001.

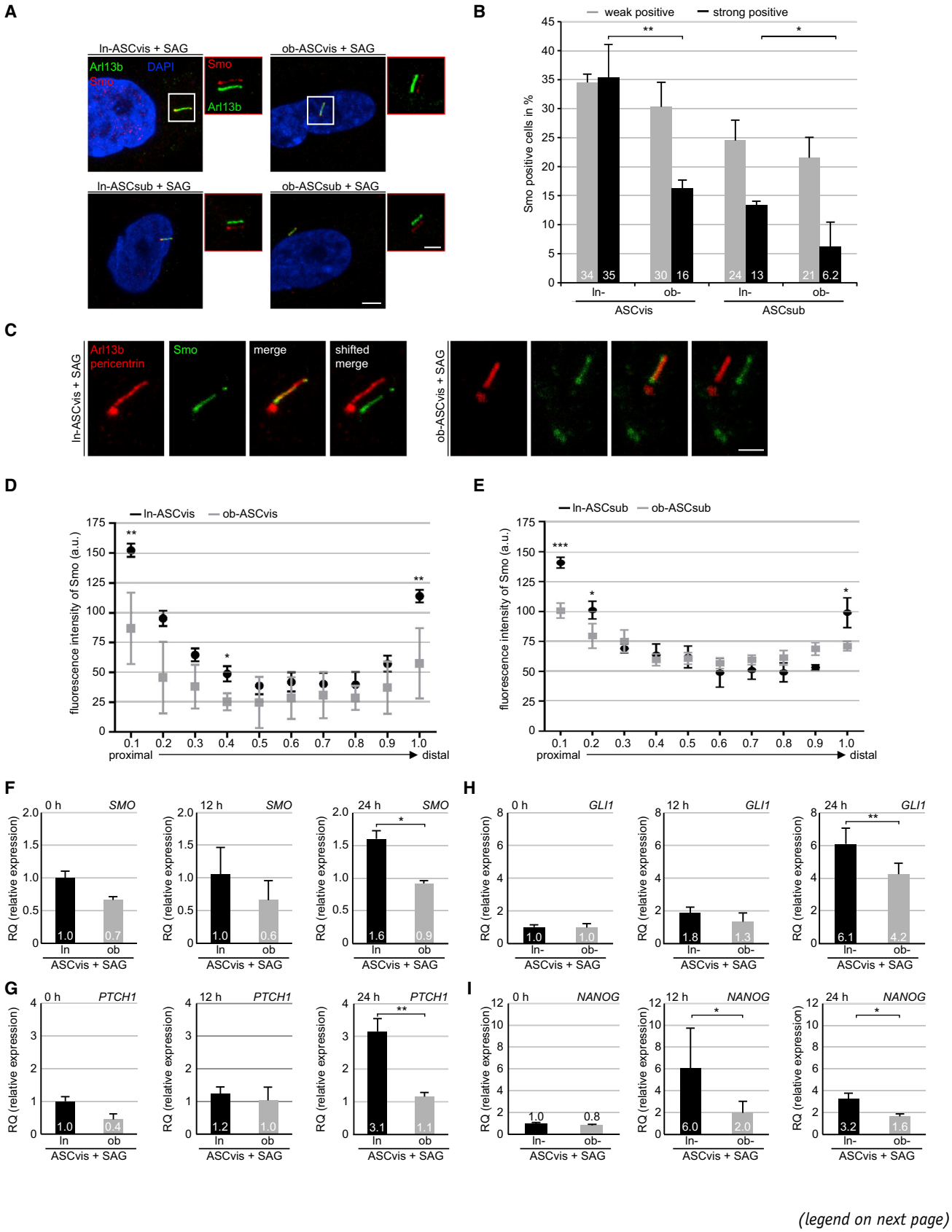

(legend on next page)

if the Hh signaling is functional in ob-ASCs, ASCs were treated with SAG, a *S*mo agonist, to activate the pathway, and stained for Smo and Arl13b followed by microscopic evaluation. In the absence of SAG, Smo was not localized to cilia of ln-ASCs and ob-ASCs. Treatment of SAG induced ciliary Smo accumulation (Figure 4A). To precisely define this, the Smo accumulation was divided into a strong (a.u. $\geq$50) and a weak group (a.u. <50). Visceral ln-ASCs responded actively to SAG by showing 34% weak and 35% strong staining of ciliary Smo (Figure 4B). Although the weak staining was comparable, visceral ob-ASCs showed only 16% strong ciliary Smo signals (Figure 4B), half of that in ln-ASCs. Although the response of subcutaneous ASCs was not as intense as in visceral ASCs (Figure 4B), subcutaneous ob-ASCs responded to SAG significantly less than ln-ASCs (Figure 4B). To study this issue in depth, line-scan analysis of fluorescent Smo was performed from the proximal base to the distal tip of cilia in visceral ln-ASCs (Figure 4C, left) and ob-ASCs (Figure 4C, right) treated with SAG and strongly stained (a.u. $\geq$50). The results revealed that, even in the strongly stained ob-ASCs, the Smo intensity was lower than in ln-ASCs, especially at the axonemal base as well as on its tip, where the differences are highly significant (Figures 4D and 4E). These data indicate that the recruitment of Smo to cilia is impaired in ob-ASCs.

Furthermore, total RNA was isolated from SAG-treated visceral ASCs for gene analysis. The Hh-related genes *SMO* and *PTCH1* (protein patched homolog 1) were lower in visceral ob-ASCs than in ln-ASCs (Figures 4F and 4G). Upon SAG stimulation, the gene expression of *SMO*, *PTCH1*, and *GLI1* was increased in visceral ln-ASCs, especially at 24 hr, whereas it was altered less in visceral ob-ASCs (Figures 4F–4H). Interestingly, *NANOG*, a direct target of the Hh pathway (Po et al., 2010), was enhanced in visceral ln-ASCs, in particular after 12 hr treatment with SAG, whereas the increase was significantly reduced in visceral ob-ASCs (Figure 4I). Comparable results were also obtained in subcutaneous ASCs (Figure S3F). These findings suggest that the Hh pathway is deficient in ob-ASCs.

Hypoxia, TNF-α, and IL-6 Reduce the Cilium Length in ln-ASCs

Obesity is characterized by hypoxia and increased pro-inflammatory factors like TNF-α and IL-6 (Donohoe et al., 2017). Murine bone marrow stromal cells have been reported to lose their cilia upon subjection to hypoxia (Proulx-Bonneau and Annabi, 2011). To test this, ln-ASCs were cultured under low oxygen tension (1.2% O_2) and stained for evaluation. Both subcutaneous and visceral ln-ASCs reduced significantly their cilium length in a time-dependent manner (Figure 5A). The cilium length started to shorten at 24 hr and further decreased during the time period up to 96 hr in visceral ln-ASCs (Figure 5B, top) and in subcutaneous ln-ASCs as well (Figure 5B, bottom). In fact, ln-ASCs incubated under hypoxia for 72 to 96 hr shortened their cilium length to the extent (Figures S4A and S4C) observed in ob-ASCs (Figure S1A). The ciliated population was also declined upon exposure to hypoxia in visceral ln-ASCs (Figure 5C) as well as in subcutaneous ln-ASCs (Figure 5D). Of note, the G2/M populations were hardly altered throughout the 96 hr period of low oxygen exposure in visceral (Figure S4B) and subcutaneous ASCs (Figure S4D). In addition, the gene levels of mitosis/deciliation-related regulators like *AURKA*, *PLK1*, *KIF2A*, and *KIF24* were actually declined (Figures S4E and S4F). These data underline the notion that shortening of cilia under hypoxia is not linked to increased cell-cycle progression.

To define the effect of TNF-α, ln-ASCs were treated with its increasing concentrations for 24 hr and stained for microscopic evaluation. Upon treatment, the cilium length in subcutaneous and visceral ln-ASCs became reduced compared with non-treated ln-ASCs (Figure S5A). The populations of ciliated cells were also declined in both types of ln-ASCs treated with TNF-α (Figure S5B). Cilia were significantly shorter in the presence of even 1 ng/mL of TNF-α in both types of ln-ASCs (Figure 5E). In addition, 58% visceral and 72% subcutaneous ln-ASCs displayed cilia with 2–4 μm length after treatment with TNF-α for 24 hr (Figure S5C).

Figure 4. Deficient Hh Pathway in ob-ASCs

(A) ASCs were treated with 200 nM SAG for 24 hr and stained as indicated. Representatives are shown. Scale bar: 4.5 μm. Insets depict shifted overlays. Scale bar: 3 μm.

(B) The Smo staining is divided into strong ($\geq$50 a.u.) and weak positive groups (<50 a.u.). The results are from three experiments (n = 200 cells for each condition) and presented as mean ± SEM.

(C) Representative cilia for measurements are shown. Scale bar: 3 μm.

(D and E) Fluorescence intensities of Smo strong staining ($\geq$50 a.u.) are shown for ASCs treated with SAG for 24 hr. Each point of the curve represents the mean fluorescence intensity (mean ± SEM) based on three experiments (n = 30 cilia) in visceral (D) and in subcutaneous ASCs (E).

(F–I) The gene levels of *SMO* (F), *PTCH1* (G), *GLI1* (H), and *NANOG* (I) are shown for ASCs treated with 200 nM SAG for 0, 12, and 24 hr. The results are from three to five experiments, presented as mean ± SEM.

Student's t test for (B) and (F)–(I). Unpaired Mann-Whitney U test for (D) and (E). *p < 0.05, **p < 0.01, ***p < 0.001.

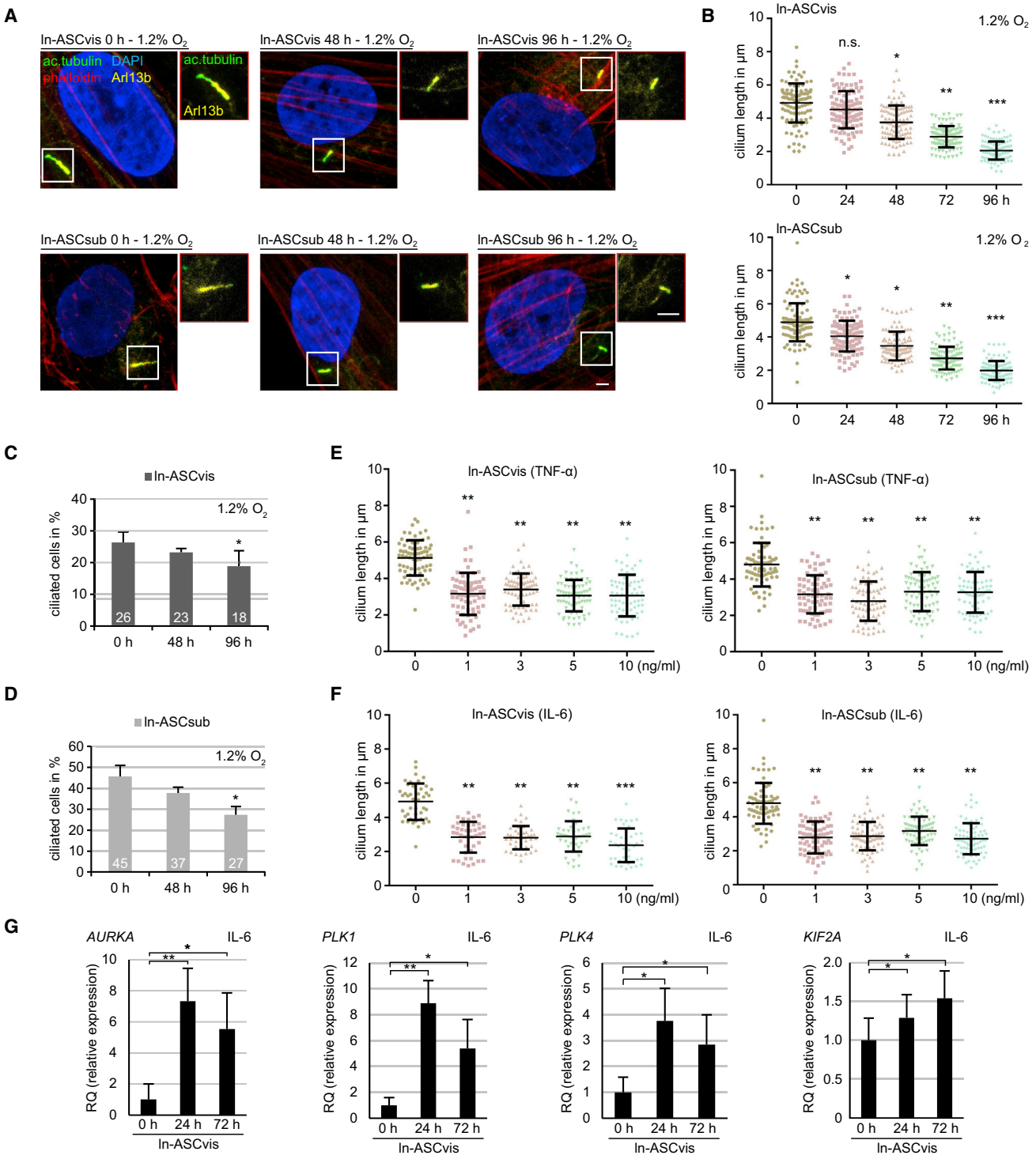

Figure 5. Hypoxia, TNF-α, and IL-6 Reduce the Cilium Length of In-ASCs

(A) In-ASCs were cultured under hypoxia (1.2% O_2) for up to 96 hr and stained as indicated. Representatives are shown. Insets: magnified boxes. Scale bars: 3 µm.

(B) Quantification of the cilium length in visceral In-ASCs (top) and subcutaneous In-ASCs (bottom) cultured under hypoxia. The results are from three experiments (n = 108–113 cilia for each condition) and presented as mean ± SEM in scatter dot plots.

(legend continued on next page)

ln-ASCs were also treated with increasing concentrations of IL-6 and stained for cilium markers. Again, the ciliary length in both types of ln-ASCs was decreased after treatment with IL-6, compared with non-treated ln-ASCs (Figures 5F and S5D). Intriguingly, while subcutaneous ln-ASCs reduced their ciliated population in the presence of IL-6, the number of ciliated cells was slightly increased in visceral ln-ASCs (Figure S5E), implying that the response to IL-6 could vary between subcutaneous and visceral ASCs. Nevertheless, further analysis displayed that the cilium length was significantly reduced in the presence of IL-6 and the peak of 4–6 μm shifted to 2–4 μm in both types of ln-ASCs (Figure S5F). Interestingly, *AURKA, PLK1, PLK4*, and *KIF2A* were greatly increased in IL-6-treated ln-ASCs (Figure 5G), as observed in ob-ASCs (Figure 2J). These results indicate that, like TNF-α, IL-6 shortens the cilium length of lean ASCs.

Impaired Hh Signaling and Reduced Differentiation in IL-6-Treated ln-ASCs

To examine if IL-6 affected the Hh pathway, IL-6-treated ln-ASCs were stimulated with SAG and stained for evaluation. Compared with non-treated ln-ASCs (Figure 6A, left), IL-6-treated ln-ASCs displayed a weaker Smo signal at shortened cilia (Figure 6A, right). The line-scan analysis demonstrated reduced Smo intensities in IL-6-treated ln-ASCs (Figure 6B). Moreover, the Hh-related genes *GLI1*, *PTCH1*, and *SMO* and its target gene *NANOG* were reduced (Figure 6C), indicative of the impairment of the Hh pathway in IL-6-treated ln-ASCs. To test if IL-6 affects the differentiation capability, IL-6-treated ln-ASCs were subjected to osteogenic differentiation medium for 14 days and stained with alizarin red S. Relative to non-treated ln-ASCs, IL-6-treated ln-ASCs showed a reduced differentiation capability (Figure 6D), as ob-ASCs (Figures 3B and 3D). In support of this, the osteogenic gene *RUNX2* (Xu et al., 2015) and osteogenesis-related gene *PTCH1* (Oliveira et al., 2012) were significantly decreased in IL-6-treated ln-ASCs (Figure 6E). These results strengthen the notion that cilia in lean ASCs could become obesity-like in the presence of obesity-associated factors like IL-6.

Inhibition of Aurora A or HDAC6 Rescues Cilia in ob-ASCs and IL-6-Treated ln-ASCs

The Aurora A gene is directly activated by c-myc via IL-6/JAK2/STAT3 signaling (Sumi et al., 2011). To test if Aurora A is a responsible factor for ciliary shortening, ob-ASCs were treated with MLN8054, a small-molecule inhibitor of Aurora A, at a low concentration range (5–15 nM), which interfered scarcely with cell-cycle progression (Figures S6C and S6D). Indeed, cilia extended their length upon MLN8054 treatment in a dose-dependent manner (Figures S6A and S6B) and restored themselves in ob-ASCs with 15 nM at 24 hr (Figure S6E). The ciliary length in treated ob-ASCs was increased by 51.9% relative to non-treated ob-ASCs (4.01 versus 2.64 μm) (Figures 7A and 7B). Moreover, MLN8054 restored shortened cilia in IL-6-treated ln-ASCs (Figures 7C and 7D). Aurora A phosphorylates and activates HDAC6 to disassemble MTs of the primary cilium (Goto et al., 2016; Malicki and Johnson, 2017). To examine the effect of HDAC6, ob-ASCs were treated with tubacin, a specific inhibitor of HDAC6. Cilia in tubacin-treated ob-ASCs were indeed prolonged (Figures S6F and S6G). The cilium length was increased by 32.2% compared with non-treated ob-ASCs (3.74 versus 2.83 μm) (Figure 7E). Like MLN8054, tubacin extended the cilium length in IL-6-treated ln-ASCs (Figure 7F). Moreover, treatment with MLN8054 or tubacin rescued the motility of ob-ASCs (Figure 7G). These data clearly suggest that Aurora A is one of the major effectors of IL-6 responsible for shortening cilia of ASCs.

DISCUSSION

We show that primary cilia are deficient in ob-ASCs and impair ASC functions, in addition to the observation that ob-ASCs produce less anti-inflammatory adipokine adiponectin after adipogenic differentiation but more pro-inflammatory cytokines like IL-6 and TNF-α contributing to the pathogenesis of obesity (Badimon and Cubedo, 2017; Strong et al., 2015). We show that cilia are shortened in isolated ob-ASCs as well as in primary obese adipose tissues. These cilia in ob-ASCs are non-dynamic and unable to

(C and D) Evaluation of ciliated visceral (C) and subcutaneous ASCs (D) cultured under hypoxia. The results are from three experiments (n = 300 cells for each time point) and shown as mean ± SEM.

(E) ln-ASCs were treated with increasing concentrations of TNF-α for 24 hr and stained for the evaluation of the cilium length in visceral (left) and subcutaneous ln-ASCs (right). The results are from three experiments (n = 79–85 cilia for each condition and in each group) and presented as mean ± SEM in scatter dot plots.

(F) ln-ASCs were treated with increasing concentrations of IL-6 for 24 hr and stained for the evaluation of the cilium length in visceral ASCs (left) and subcutaneous ASCs (right). The results are from three experiments (n = 73–80 cilia for each condition in each group) and presented as mean ± SEM in scatter dot plots.

(G) The gene levels of deciliation molecules are shown in visceral ln-ASCs treated with 5 nM IL-6 for 72 hr. The results are based on three independent experiments and presented as mean ± SEM.

Unpaired Mann-Whitney U test for (B), (E), and (F). Student's t test for (C), (D), and (G). *p < 0.05, **p < 0.01, ***p < 0.001.

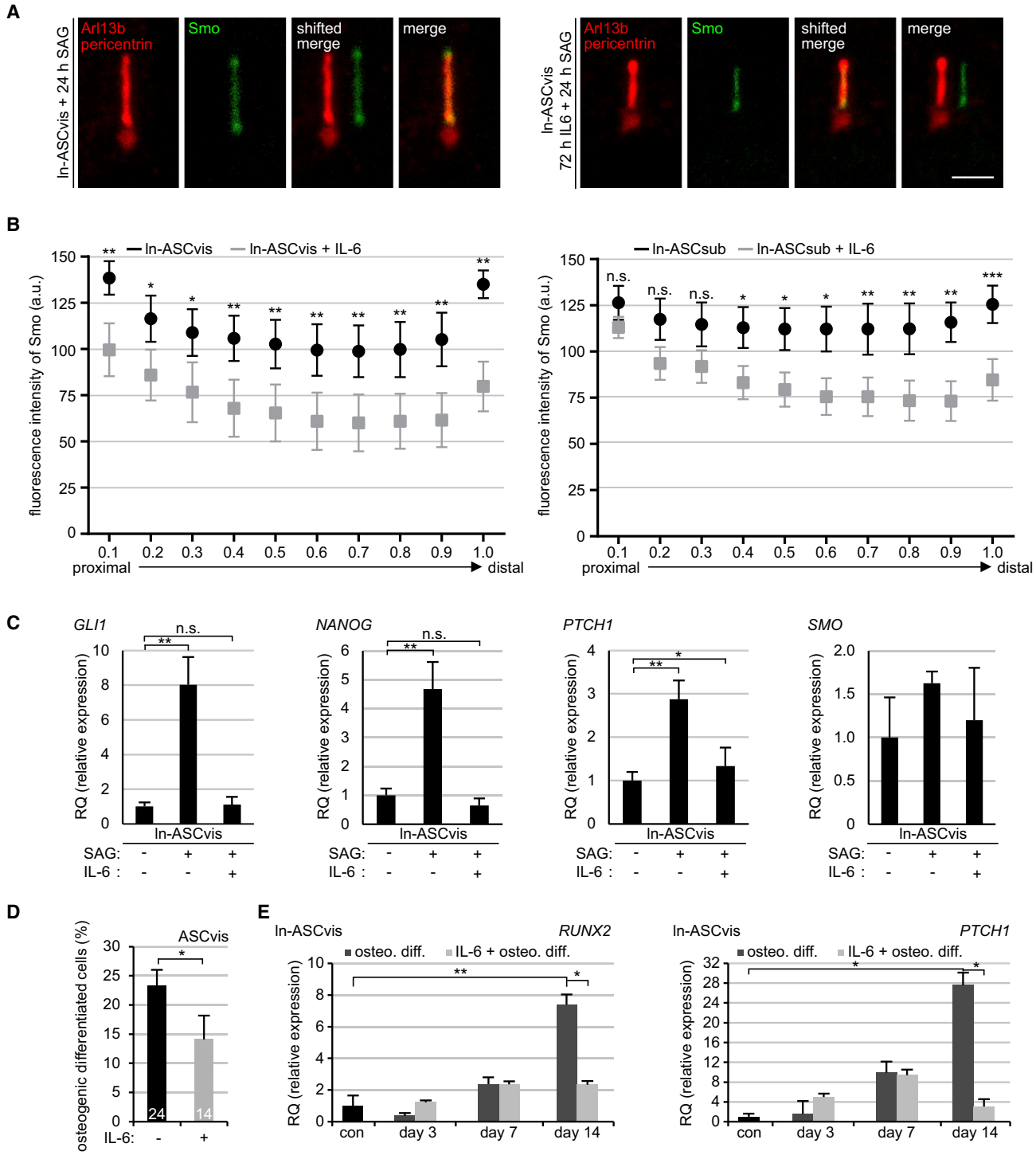

Figure 6. Impaired Hh Signaling and Decreased Differentiation in IL-6-Treated ln-ASCs

(A) Visceral ln-ASCs were treated with IL-6 (5 ng/mL, 72 hr), followed by stimulation with SAG (200 nM, 24 hr), and stained as indicated. Representative cilia are shown. Left: cilium in control ln-ASC. Right: cilium in IL-6-treated ln-ASC. Scale bar: 3 μm.

(B) The fluorescence intensity of axonemal Smo (green channel) was measured from the axonemal base to its distal tip in non- and IL-6-treated visceral (left) and subcutaneous ln-ASCs (right). Each point of the curve represents the mean fluorescence intensity (mean ± SEM, n = 30 cilia in each condition, pooled from three experiments).

(legend continued on next page)

respond properly to intracellular as well as extracellular cues. ob-ASCs with shortened cilia display a defective Hh pathway, migrate slowly, and differentiate poorly. These data strongly suggest that deficient primary cilia, induced secondarily by obesity-related factors, are not fully functional as sensors and transducers of environmental signals, which could reduce ASC activities and worsen diseased adipose tissues in obesity.

The cilium length is regulated by numerous pathways (Sanchez and Dynlacht, 2016) and is tightly coupled with the cell cycle (Malicki and Johnson, 2017). Crucial mitotic regulators like Aurora A and Plk1 serve as deciliation molecules by promoting ciliary disassembly or blocking its prolongation (Sanchez and Dynlacht, 2016). We show a comparable proliferation rate as well as mitotic index between ln- and ob-ASCs, suggesting that shortened cilia in ob-ASCs are not the consequence of enhanced cell-cycle progression. Intriguingly, the genes *AURKA*, *PLK1*, *PLK4*, *KIF2A*, and *KIF24* are increased in ob-ASCs. We assume that the increased amounts of these deciliation molecules are sufficient for shortening cilia or blocking their prolongation and yet not enough for stimulating the cell cycle. Alternatively, the coupling machinery for correlating ciliogenesis with the cell cycle is disrupted in these ASCs undergoing a long term of subclinical inflammation.

Hh signaling, an evolutionarily conserved pathway responsible for embryonic development and stem cell maintenance (Bodle and Loboa, 2016; He et al., 2017; Pak and Segal, 2016), is dysfunctional in ob-ASCs. This is evidenced by hampered recruitment of Smo to cilia and impaired transcriptional activation of *SMO*, *PTCH1*, and *GLI1* upon SAG stimulation. The defective Hh pathway possibly explains failures in differentiation and migration of ob-ASCs.

Obesity is commonly characterized by hypoxia and increased pro-inflammatory milieu (Ibrahim, 2010). We show that, compared with ln-ASCs, ob-ASCs secrete much more IL-6 and TNF-α, which, via paracrine/autocrine pathways, could impact the development of obesity. Indeed, hypoxia, TNF-α, or IL-6 reduces the cilium length of ln-ASCs to the size observed in ob-ASCs. Like obese ASCs, IL-6-treated ln-ASCs display an impaired Hh pathway, a reduced differentiation capability, and an enhanced gene expression of deciliation molecules. IL-6 targets numerous downstream genes by activating the signal transducer and activator of transcription 3 (STAT3), the mitogen-activated protein kinase (MAPK), and phosphatidylinositol 3-kinase (PI3K) signaling as well (Junk et al., 2014). Aurora A, a crucial regulator for the cilium disassembly (Sanchez and Dynlacht, 2016), is directly targeted by the IL-6/JAK2/STAT3 cascade via c-myc (Sumi et al., 2011). We show that inhibition of Aurora A or its target HDAC6 rescues the cilium length in ob-ASCs and in IL-6-treated ln-ASCs as well. These important findings highlight that Aurora A is one of the critical downstream targets activated by IL-6. Based on these data, we may suggest that obesity-associated factors induce ciliary defects possibly by affecting the ASC transcriptome, via multiple signaling pathways like JAK/STAT, PI3K, and MAPK, facilitating the gene expression of deciliation molecules like Aurora A.

While patients with ciliopathies such as the Bardet-Biedl syndrome suffer from obesity (Vaisse et al., 2017), we show here that obesity alters the biogenesis of the primary cilium in ASCs, suggestive of an intrinsic correlation between ciliogenesis and adipogenesis (Vaisse et al., 2017; Volta and Gerdes, 2017). Impaired ASCs may affect the pathogenesis of obesity as suggested (Badimon and Cubedo, 2017), and the mechanisms underlying this ASC impairment in obesity are, however, not defined. We show here that obesity-related factors directly shorten cilia and compromise their function, which lowers the differentiation potential of ASCs, resulting in adipocyte hypertrophy and defective homeostasis. Moreover, ASCs with dysfunctional cilia exhibit hindered motility, indicative of their incapability of functioning in distant sites. Importantly, ASCs are involved in anti-inflammation and immunomodulation by inhibiting natural killer cell activation (DelaRosa et al., 2012) and reducing proliferation and function of B cells (Bochev et al., 2008). It is tempting to suggest that ob-ASCs with defective cilia are unable to modulate the immune system, worsening local and systemic inflammation in obese patients.

In conclusion, we show that, in addition to deregulated secretion of adipokines, ob-ASCs have shortened and deficient cilia, triggered by increased ciliary disassembly regulators like Aurora A induced by obesity-associated factors. Impaired cilia compromise ASC functionalities, leading possibly to defective adipogenesis, adipocyte hypertrophy,

(C) The gene levels of *GLI1*, *NANOG*, *PTCH1*, and *SMO* are shown for visceral ln-ASCs treated as in (A). The results are based on three experiments and presented as mean ± SEM.

(D) Visceral ln-ASCs were treated or not with IL-6 (5 ng/mL, 72 hr) and subjected to osteogenic differentiation (osteo. diff.) for 14 days. Differentiation rate was quantified by evaluating alizarin red S staining. The results are presented as mean ± SEM (n = 300 cells for each condition, pooled from three independent experiments).

(E) The gene levels of *RUNX2* and *PTCH1* are shown for visceral ln-ASCs treated as in (D). The results are based on three individual experiments and presented as mean ± SEM.

Unpaired Mann-Whitney U test for (B). Student's t test for (C)–(E). *p < 0.05, **p < 0.01, ***p < 0.001.

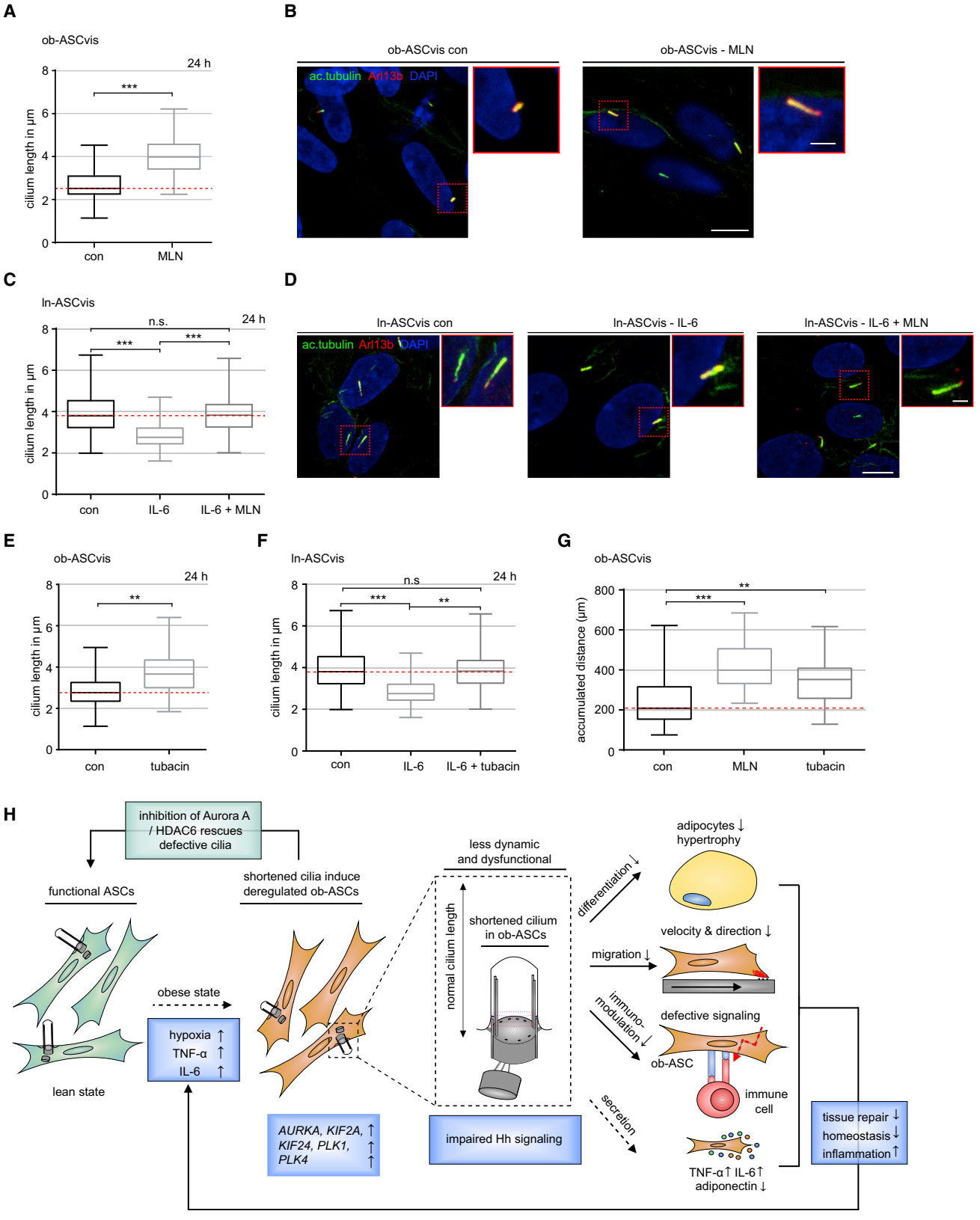

(legend on next page)

hypoxia, and deregulated immunomodulation, well-known phenomena observed in obese adipose tissues (Figure 7H). Although being secondary, impairment of primary cilia in ASCs may be a key event for the determination of the fate of obesity. Further *in vivo* studies are required to explore the clinical significance of ciliogenesis in the development of obesity. It is also important to determine if or how other obesity-related factors like leptin and metabolites affect primary cilia of ASCs.

EXPERIMENTAL PROCEDURES

Human ASC Isolation, Surface Markers by Flow Cytometry, and Reagents

This work was approved by the Ethics Committee of the Johann Wolfgang Goethe University Hospital Frankfurt, and informed written consent was obtained from all donors. Visceral (omental) and subcutaneous (abdominal) adipose tissues were taken from women undergoing cesarean section. Donor information is listed in Table S1. ASC isolation, culture, and purity evaluation are detailed in Supplemental Experimental Procedures.

FACSCalibur (BD Biosciences, Heidelberg) was used for determining the ASC surface makers. Cells were harvested with 0.25% trypsin and fixed for 15 min with ice-cold 2% paraformaldehyde at 4°C. Cells were washed twice with flow cytometry buffer (PBS with 0.2% Tween 20 and 2% fetal calf serum [FCS]) and stained with antibodies described in Supplemental Experimental Procedures.

IL-6 and TNF-α were from PeproTech (Hamburg). Aurora A inhibitor MLN8054 and HDAC6 inhibitor tubacin were from Sigma-Aldrich (Taufkirchen) and Selleckchem (Munich), respectively.

Depolymerization Assays, SAG Stimulation, Cell Viability, and Cell-Cycle Analysis

For depolymerization assay of axonemal MTs, cells were subjected to 10 μM nocodazole (Sigma-Aldrich) or cold treatment for 30 min for immunofluorescence staining described below. Cells were incubated with 200 nM SAG (Bioscience, Wiesbaden) in the absence of FCS to activate the Hh pathway for further analysis.

Cell-viability assays were performed by using Cell Titer-Blue cell-viability assay (Promega, Mannheim) as described (Kreis et al., 2015). ASCs were seeded with 3,000 cells per 96-well plate and cell proliferation was measured up to 96 hr. The cell-cycle distribution was analyzed using a FACSCalibur (BD Biosciences), as reported (Muschol-Steinmetz et al., 2013, 2016). Briefly, cells were harvested, washed with PBS, fixed in chilled 70% ethanol at 4°C for 30 min, treated with 1 mg/mL RNase A (Sigma-Aldrich), and stained with 100 μg/mL propidium iodide for 30 min at 37°C. DNA content was determined.

ASC Differentiation and Western Blot Analysis

ASC differentiation was performed as reported (Ritter et al., 2015). To induce adipogenic differentiation, ASCs were cultured with StemMACS AdipoDiff media (Miltenyi Biotec, Gladbach) up to 14 days. Cells were then fixed and stained for oil red O and adiponectin (Abcam, Cambridge, #AB22554) characteristic of adipocytes. For osteogenic differentiation, ASCs were incubated in StemMACS OsteoDiff media (Miltenyi Biotec) up to 21 days, fixed, and stained with 2% alizarin red S (pH 4.2) to visualize calcific deposition by cells of an osteogenic lineage.

Western blot analysis was performed as reported (Muschol-Steinmetz et al., 2016; Steinhauser et al., 2017), using mouse monoclonal antibodies against cyclin B1 (#sc-752) and β-actin (#sc-47778) from Santa Cruz Biotechnology (Heidelberg).

Immunofluorescence Staining and Measurement, Immunohistochemistry, and Cell-Motility Evaluation

Immunofluorescence staining and motility evaluation were performed as described (Ritter et al., 2015) and described in detail in Supplemental Experimental Procedures.

Figure 7. Inhibition of Aurora A or HDAC6 Rescues the Cilium Length in ob-ASCs and IL-6-Treated ln-ASCs

(A and B) Visceral ob-ASCs were treated with the Aurora A inhibitor MLN8054 (MLN; 15 nM, 24 h) and stained for the evaluation of the cilium length. The results are based on three experiments (n = 180 cilia for each group) (A). Representatives are shown in (B). Scale bar: 10 μm. Inset scale bar: 2 μm.

(C and D) Visceral ln-ASCs were treated with IL-6 (5 ng/mL, 24 hr), followed by addition of MLN8054 (15 nM, 24 hr), and stained for evaluation. The results are from three experiments (n = 180 cilia for each condition) (C). Representatives are shown in (D). Scale bar: 10 μm. Inset scale bar: 2 μm.

(E) Visceral ob-ASCs were treated with the HDAC6 inhibitor tubacin (26 nM, 24 hr) and stained for evaluation. The results are based on three experiments (n = 180 cilia for each condition).

(F) Visceral ln-ASCs were treated with IL-6 (5 ng/mL, 24 hr), followed by addition of tubacin (26 nM, 24 hr), and stained for evaluation. The results are from three experiments (n = 180 cilia for each condition).

(G) Visceral ob-ASCs treated with MLN8054 (15 nM, 24 hr) or tubacin (26 nM, 24 hr) were subjected to time-lapse microscopy for analyzing their motility. The accumulated distance of non-, MLN8054-, or tubacin-treated ob-ASCs is shown (n = 87 cells for each condition, pooled from three experiments).

(H) Schematic illustration of the proposed working model. Obesity-associated factors shorten primary cilia in obese ASCs, which renders these cells dysfunctional, causing defects in differentiation, angiogenesis, tissue repair, and immunomodulation.

Box and whisker plots were used to show the median and the minimal to maximal range of the values and red dashed line indicates the cilium median length of control ASCs in (A), (C), and (E)–(G). Unpaired Mann-Whitney U test for (A), (C), and (E)–(G). $^{**}p < 0.01$, $^{***}p < 0.001$.

Adipokine Evaluation via ELISA, RNA Extraction, and Real-Time PCR

Seventy-two hour supernatants were collected before and after differentiation for evaluating IL-6 and TNF-α (PeproTech, Hamburg) and adiponectin (Sigma-Aldrich) via ELISA as instructed by the manufacturers. Quantitative gene level was measured as reported (Muschol-Steinmetz et al., 2013), detailed in Supplemental Experimental Procedures.

Statistical Analysis

Student's t test (two tailed and paired or homoscedastic) was used to evaluate the significant difference between diverse groups for gene analysis, cell-viability assay, cell-cycle distribution, and ciliated-cell population. The statistical evaluation of the single-cell tracking assay, line-scan analysis, and measurement of the cilium length was performed by using an unpaired Mann-Whitney U test (two tailed). Difference was considered as statistically significant when $p < 0.05$.

SUPPLEMENTAL INFORMATION

Supplemental Information includes Supplemental Experimental Procedures, six figures, and two tables and can be found with this article online at https://doi.org/10.1016/j.stemcr.2017.12.022.

AUTHOR CONTRIBUTIONS

F.L. and J.Y. conceived and supervised the project. J.Y. and A.R. designed the experiments. A.R., A.F., N.N.K., S.R., and S.C.H. performed experiments and analyzed data. U.K.K., D.B., and C.S. collected samples. J.Y. wrote the manuscript. All authors did critical reading and modified the manuscript.

ACKNOWLEDGMENTS

This project is partially supported by the Verein zur Förderung der Reproduktiven Gesundheit im Alter E.V. We are grateful to our patients for making this study possible. We thank Drs. He and Anderson, Sloan-Kettering Institute, for kindly providing us the ImageJ plug-in Plot Roi Profile for analyzing the fluorescence intensity in cilia.

Received: August 2, 2017
Revised: December 28, 2017
Accepted: December 28, 2017
Published: January 25, 2018

REFERENCES

Badimon, L., and Cubedo, J. (2017). Adipose tissue depots and inflammation: effects on plasticity and resident mesenchymal stem cell function. Cardiovasc. Res. *113*, 1064–1073.

Bochev, I., Elmadjian, G., Kyurkchiev, D., Tzvetanov, L., Altankova, I., Tivchev, P., and Kyurkchiev, S. (2008). Mesenchymal stem cells from human bone marrow or adipose tissue differently modulate mitogen-stimulated B-cell immunoglobulin production in vitro. Cell Biol. Int. *32*, 384–393.

Bodle, J.C., and Loboa, E.G. (2016). Concise review: primary cilia: control centers for stem cell lineage specification and potential targets for cell-based therapies. Stem Cells *34*, 1445–1454.

Cawthorn, W.P., Scheller, E.L., and MacDougald, O.A. (2012). Adipose tissue stem cells: the great WAT hope. Trends Endocrinol. Metab. *23*, 270–277.

Dalbay, M.T., Thorpe, S.D., Connelly, J.T., Chapple, J.P., and Knight, M.M. (2015). Adipogenic differentiation of hMSCs is mediated by recruitment of IGF-1r onto the primary cilium associated with cilia elongation. Stem Cells *33*, 1952–1961.

DelaRosa, O., Sanchez-Correa, B., Morgado, S., Ramirez, C., del, R.B., Menta, R., Lombardo, E., Tarazona, R., and Casado, J.G. (2012). Human adipose-derived stem cells impair natural killer cell function and exhibit low susceptibility to natural killer-mediated lysis. Stem Cells Dev. *21*, 1333–1343.

Dominici, M., Le, B.K., Mueller, I., Slaper-Cortenbach, I., Marini, F., Krause, D., Deans, R., Keating, A., Prockop, D., and Horwitz, E. (2006). Minimal criteria for defining multipotent mesenchymal stromal cells. The International Society for Cellular Therapy position statement. Cytotherapy *8*, 315–317.

Donohoe, C.L., Lysaght, J., O'Sullivan, J., and Reynolds, J.V. (2017). Emerging concepts linking obesity with the hallmarks of cancer. Trends Endocrinol. Metab. *28*, 46–62.

Forcioli-Conti, N., Esteve, D., Bouloumie, A., Dani, C., and Peraldi, P. (2016). The size of the primary cilium and acetylated tubulin are modulated during adipocyte differentiation: analysis of HDAC6 functions in these processes. Biochimie *124*, 112–123.

Forcioli-Conti, N., Lacas-Gervais, S., Dani, C., and Peraldi, P. (2015). The primary cilium undergoes dynamic size modifications during adipocyte differentiation of human adipose stem cells. Biochem. Biophys. Res. Commun. *458*, 117–122.

Freitas Lima, L.C., Braga, V.A., do Socorro de Franca Silva, M., Cruz, J.C., Sousa Santos, S.H., de Oliveira Monteiro, M.M., and Balarini, C.M. (2015). Adipokines, diabetes and atherosclerosis: an inflammatory association. Front. Physiol. *6*, 304.

Gimble, J.M., Katz, A.J., and Bunnell, B.A. (2007). Adipose-derived stem cells for regenerative medicine. Circ. Res. *100*, 1249–1260.

Goto, H., Inaba, H., and Inagaki, M. (2016). Mechanisms of ciliogenesis suppression in dividing cells. Cell Mol. Life Sci. *74*, 881–890.

He, M., Agbu, S., and Anderson, K.V. (2017). Microtubule motors drive hedgehog signaling in primary cilia. Trends Cell Biol. *27*, 110–125.

He, M., Subramanian, R., Bangs, F., Omelchenko, T., Liem, K.F., Jr., Kapoor, T.M., and Anderson, K.V. (2014). The kinesin-4 protein Kif7 regulates mammalian Hedgehog signalling by organizing the cilium tip compartment. Nat. Cell Biol. *16*, 663–672.

Hilgendorf, K.I., Johnson, C.T., and Jackson, P.K. (2016). The primary cilium as a cellular receiver: organizing ciliary GPCR signaling. Curr. Opin. Cell Biol. *39*, 84–92.

Ibrahim, M.M. (2010). Subcutaneous and visceral adipose tissue: structural and functional differences. Obes. Rev. *11*, 11–18.

Janke, C., and Bulinski, J.C. (2011). Post-translational regulation of the microtubule cytoskeleton: mechanisms and functions. Nat. Rev. Mol. Cell Biol. *12*, 773–786.

Junk, D.J., Bryson, B.L., and Jackson, M.W. (2014). HiJAK'd signaling; the STAT3 paradox in senescence and cancer progression. Cancers (Basel) *6*, 741–755.

Kloting, N., and Bluher, M. (2014). Adipocyte dysfunction, inflammation and metabolic syndrome. Rev. Endocr. Metab. Disord. *15*, 277–287.

Korobeynikov, V., Deneka, A.Y., and Golemis, E.A. (2017). Mechanisms for nonmitotic activation of Aurora-A at cilia. Biochem. Soc. Trans. *45*, 37–49.

Kreis, N.N., Louwen, F., Zimmer, B., and Yuan, J. (2015). Loss of p21Cip1/CDKN1A renders cancer cells susceptible to Polo-like kinase 1 inhibition. Oncotarget *6*, 6611–6626.

Malicki, J.J., and Johnson, C.A. (2017). The cilium: cellular antenna and central processing unit. Trends Cell Biol. *27*, 126–140.

Muschol-Steinmetz, C., Friemel, A., Kreis, N.N., Reinhard, J., Yuan, J., and Louwen, F. (2013). Function of survivin in trophoblastic cells of the placenta. PLoS One *8*, e73337.

Muschol-Steinmetz, C., Jasmer, B., Kreis, N.N., Steinhauser, K., Ritter, A., Rolle, U., Yuan, J., and Louwen, F. (2016). B-cell lymphoma 6 promotes proliferation and survival of trophoblastic cells. Cell Cycle *15*, 827–839.

Ng, L.W., Yip, S.K., Wong, H.K., Yam, G.H., Liu, Y.M., Lui, W.T., Wang, C.C., and Choy, K.W. (2009). Adipose-derived stem cells from pregnant women show higher proliferation rate unrelated to estrogen. Hum. Reprod. *24*, 1164–1170.

O'Neill, S., and O'Driscoll, L. (2015). Metabolic syndrome: a closer look at the growing epidemic and its associated pathologies. Obes. Rev. *16*, 1–12.

Oliveira, F.S., Bellesini, L.S., Defino, H.L., da Silva Herrero, C.F., Beloti, M.M., and Rosa, A.L. (2012). Hedgehog signaling and osteoblast gene expression are regulated by purmorphamine in human mesenchymal stem cells. J. Cell Biochem. *113*, 204–208.

Pachon-Pena, G., Yu, G., Tucker, A., Wu, X., Vendrell, J., Bunnell, B.A., and Gimble, J.M. (2011). Stromal stem cells from adipose tissue and bone marrow of age-matched female donors display distinct immunophenotypic profiles. J. Cell Physiol. *226*, 843–851.

Pak, E., and Segal, R.A. (2016). Hedgehog signal transduction: key players, oncogenic drivers, and cancer therapy. Dev. Cell *38*, 333–344.

Patel, P., and Abate, N. (2013). Body fat distribution and insulin resistance. Nutrients *5*, 2019–2027.

Po, A., Ferretti, E., Miele, E., De, S.E., Paganelli, A., Canettieri, G., Coni, S., Di, M.L., Biffoni, M., Massimi, L., et al. (2010). Hedgehog controls neural stem cells through p53-independent regulation of Nanog. EMBO J. *29*, 2646–2658.

Proulx-Bonneau, S., and Annabi, B. (2011). The primary cilium as a biomarker in the hypoxic adaptation of bone marrow-derived mesenchymal stromal cells: a role for the secreted frizzled-related proteins. Biomark. Insights *6*, 107–118.

Ritter, A., Friemel, A., Fornoff, F., Adjan, M., Solbach, C., Yuan, J., and Louwen, F. (2015). Characterization of adipose-derived stem cells from subcutaneous and visceral adipose tissues and their function in breast cancer cells. Oncotarget *6*, 34475–34493.

Sanchez, I., and Dynlacht, B.D. (2016). Cilium assembly and disassembly. Nat. Cell Biol. *18*, 711–717.

Serena, C., Keiran, N., Ceperuelo-Mallafre, V., Ejarque, M., Fradera, R., Roche, K., Nunez-Roa, C., Vendrell, J., and Fernandez-Veledo, S. (2016). Obesity and type 2 diabetes alters the immune properties of human adipose derived stem cells. Stem Cells *34*, 2559–2573.

Steinhauser, K., Kloble, P., Kreis, N.N., Ritter, A., Friemel, A., Roth, S., Reichel, J.M., Michaelis, J., Rieger, M.A., Louwen, F., et al. (2017). Deficiency of RITA results in multiple mitotic defects by affecting microtubule dynamics. Oncogene *36*, 2146–2159.

Strong, A.L., Bowles, A.C., Wise, R.M., Morand, J.P., Dutreil, M.F., Gimble, J.M., and Bunnell, B.A. (2016). Human adipose stromal/stem cells from obese donors show reduced efficacy in halting disease progression in the experimental autoimmune encephalomyelitis model of multiple sclerosis. Stem Cells *34*, 614–626.

Strong, A.L., Burow, M.E., Gimble, J.M., and Bunnell, B.A. (2015). Concise review: the obesity cancer paradigm: exploration of the interactions and crosstalk with adipose stem cells. Stem Cells *33*, 318–326.

Sumi, K., Tago, K., Kasahara, T., and Funakoshi-Tago, M. (2011). Aurora kinase A critically contributes to the resistance to anti-cancer drug cisplatin in JAK2 V617F mutant-induced transformed cells. FEBS Lett. *585*, 1884–1890.

Vaisse, C., Reiter, J.F., and Berbari, N.F. (2017). Cilia and obesity. Cold Spring Harb. Perspect. Biol. *9*, a028217.

Volta, F., and Gerdes, J.M. (2017). The role of primary cilia in obesity and diabetes. Ann. N. Y. Acad. Sci. *1391*, 71–84.

Wu, J., Ivanov, A.I., Fisher, P.B., and Fu, Z. (2016). Polo-like kinase 1 induces epithelial-to-mesenchymal transition and promotes epithelial cell motility by activating CRAF/ERK signaling. Elife *5*, e10734.

Xu, J., Li, Z., Hou, Y., and Fang, W. (2015). Potential mechanisms underlying the Runx2 induced osteogenesis of bone marrow mesenchymal stem cells. Am. J. Transl. Res. *7*, 2527–2535.

Zhu, D., Shi, S., Wang, H., and Liao, K. (2009). Growth arrest induces primary-cilium formation and sensitizes IGF-1-receptor signaling during differentiation induction of 3T3-L1 preadipocytes. J. Cell Sci. *122*, 2760–2768.